Thin Solid Films 688 (2019) 137437

Contents lists available at ScienceDirect

Thin Solid Films

journal homepage: www.elsevier.com/locate/tsf

Improving the atmospheric plasma deposition of crystalline inorganic coatings

A. Remy[a], M. Serigne Fall[a], T. Segato[b], S. Godet[b], M.P. Delplancke-Ogletree[b], P. Panini[c], Y. Geerts[c], F. Reniers[a,*]

[a] Université libre de Bruxelles, Faculty of Sciences, Chemistry of Surfaces, Interfaces and Nanomaterials – ChemSIN, cp 255, Avenue F.D. Roosevelt, 50 – B-, 1050 Brussels, Belgium
[b] Université Libre de Bruxelles, 4MAT, cp 165/63, Av. F.D. Roosevelt, 50 – B-, 1050 Brussels, Belgium
[c] Université Libre de Bruxelles, Faculty of Sciences, Laboratoire de Chimie des Polymères, cp 206/01, 50-B-, 1050 Brussels, Belgium

ABSTRACT

The deposition of good quality crystalline inorganic coatings by atmospheric pressure dielectric barrier discharge remains a challenge. Thanks to an original coupling of a substrate heating device based on an inductive current loop and located under the dielectric and an atmospheric pressure dielectric barrier discharge, we show that one can deposit in one step crystalline vanadium oxide and titanium oxide, with grain sizes bigger than those achieved by post-deposition annealing.

1. Introduction

The deposition of thin films using physical vapour deposition (PVD) or plasma-enhanced chemical vapour deposition (PECVD) using low pressure plasma systems has been the subject of thousands of papers these last 40 years. Techniques such as DC-sputtering, magnetron sputtering [1], radiofrequency (RF) sputtering [2–4] or more recently HiPIMS [5] have been developed and optimized thanks to hundreds of researchers. Metallic, organic and inorganic coatings can now be deposited with an extreme reproducibility, at high speed, with controlled crystallinity. Industrial vacuum coater lines are implemented throughout all the world. The evolution of the concepts in thin film sputter deposition can be found in [6]. In this review, it is shown that the deposition of the right coating not only required the right chemistry, but also the right structure, a controlled number of defects and the right crystallinity. Because of the crucial importance of these structural parameters, research has been focused on low pressure techniques and/or techniques such as chemical vapour deposition that may use high temperature. The key concept of getting crystalline coatings and structure-controlled coatings is the energy available at the surface. This energy may be brought by the incoming particles themselves, by further resputtering of the surface, or from heating of the substrate. Appropriate surface preparation is also often required to achieve the best coating. A side parameter is also the deposition time, as a conventional approach tells us that one needs to operate at low deposition rates to obtain the best coatings. Although the contribution of our group was minor in that domain, we also could deposit epitaxial films of Ag, Pd, and AgPd alloys, Cu, Rh, Pd, CuPd and CuRh alloys [7] as well as crystalline carbide and nitride films (MoC, WC, MoN, WN, CrC [8,9]). Classically, most of such coatings that provide a significant added value to the material are deposited under vacuum, as it offers an excellent control on the remaining gas impurities, it allows tuning the energy of the particles arriving on the substrate thanks to their high mean free path, and it allows complex chemistry (oxides, carbides, nitrides, alloys, …). However, amongst main constraints are the complexity of industrial vacuum coater lines, and very often a limited deposition rate. Although these remarks must be counterbalanced by the many improvement of all the above-mentioned techniques, they are often in the back of the mind of the researchers and the coatings manufacturers. Other approaches were therefore developed, such as chemical vapour deposition (CVD), but it necessitates usually high temperatures, or sol-gel deposition, but it requires most often a high temperature post-annealing treatment to remove the solvants and to give its final texture to the coating.

Atmospheric plasmas have been used for a long time for ozone synthesis (the Siemens process dates from 1857 [10]) and for surface activation. Their main advantage is their ability to be run at atmospheric pressure, avoiding therefore the need of vacuum systems (chambers, pumps, transfer locks…). For this reason, ultrahigh speed (up to 500 m/min) surface treatment can be achieved for surface activation of materials, or for instance, for the surface cleaning of metals [11]. However, the main advantage of atmospheric plasma is also their main drawback when it comes to deposition of coatings: because they are run at atmospheric pressure, without pumping, the gas is not well

* Corresponding author.
E-mail address: freniers@ulb.ac.be (F. Reniers).

https://doi.org/10.1016/j.tsf.2019.137437
Received 1 May 2019; Received in revised form 19 July 2019; Accepted 19 July 2019
Available online 20 July 2019
0040-6090/

controlled, introducing impurities in the coatings, and the mean free path is very small, leading to incoming particles having an extremely low energy. For this reason, the first depositions were dedicated to organic coatings, to synthesize random “plasma polymers” and to the deposition of amorphous inorganic coatings in their oxide form, like SiOx, acting as barrier layers for oxygen, water or corrosion [12].

Another drawback is the presence of residual air in chambers that, for a long time, prevent researchers to deposit coatings that could be easily oxydised (like Si).

The atmospheric plasma deposition of organic coatings (often named “plasma polymers”) has been the subject of hundreds of papers and many reviews can be found in the literature [13–16]. People can deposit PVC-like polymers [17], polytetrafluororethylene-like [18], acrylates [19], biocompatible polyethylene glycol [20], super-hydrophobic [21], hydrophilic coatings [22], silane-based [23], polystyrene [24].

When it comes to crystalline inorganic coatings, for years, the main option was to perform annealing on the quasi-amorphous deposited films. Another option is the resistive heating of the substrate during deposition. This option is however often hard to realize in real experimental conditions, as most of the atmospheric plasma deposition is done using a high frequency (in the 1–100 kHz range) dielectric barrier discharge. Amongst the main problems are electrical interferences between the heating circuit and the plasma circuit, and the difficulty to heat a substrate placed on a dielectric material. Nevertheless, a few studies report successful use of a resistive heating system to deposit, for instance, TiO_2 in anatase phase [25].

We propose in this paper an original approach for heating the substrate, new for atmospheric plasma discharge, based on a secondary inductive electrical circuit placed at one of the two electrodes of a DBD, under the dielectric. This system allows, as for some of the low pressure deposition systems, to deposit crystalline inorganic coatings. Vanadium oxide and titanium oxide are selected as examples in this paper to show the feasibility of the process. They are chosen for their wide applications, and for their various crystalline forms and oxidation states. Vanadium oxides can be used for infrared sensors [26], as catalysts [27], as thermochromic or electrochromic devices [28] and as cathode for Li-ion batteries [29]. Vanadium as also 5 different oxidation states. Titanium oxide is well known as photocatalyst, where it has been shown that, in most conditions, the anatase form or a mix of rutile and anatase are the most active ones [30].

2. Experimental

The precursors used for this study are vanadium oxytriisopropoxide (VOTP) from Alfa Aesar (product # 89798 CAS # 5588-84-1) and titanium tetraisopropoxide (TTIP), from Sigma-Aldrich (Product #205273 CAS#546–68-9). They are chosen for their limited toxicity and hazardous properties and for their high vapour pressure. The precursors are introduced inside the plasma chamber by bubbling argon into the heated liquid precursors. Argon (Air Liquide P0021L50S2A001) is used as the carrier gas for the precursors, and as the main plasma gas. Oxygen (Air Liquide P0361L50R2A001) is used as secondary reactive gas. The substrates used for this study are Si wafer (N doped (001) oriented from Pi-Kem), Au (coated on glass), and Al 2024 alloy, and are selected for their appropriate properties for the characterization techniques. Before deposition, substrates were cleaned with methanol and isooctane to avoid contamination. Deposition is realized in the home made DBD chamber whose schematic is presented in Fig. 1. The power generator is an AFS G10S-*V* instrument operating at 19 kHz in our conditions. The injected power was varied from 0 to 80 W in this study.

The main parameters used for the deposition of coatings are summarized in Table 1.

Although the chemical mechanisms are complex, the two chemical reactions can be summarized as:

$$2\,VO(C_3H_7O)_3 + 54\,O \rightarrow V_2O_5 + 21\,H_2O + 18\,CO_2$$

$$Ti(OC_3H_7)_4 + 36\,O \rightarrow TiO_2 + 14\,H_2O + 12\,CO_2$$

where the atomic oxygen originates from the dissociation of O_2 in the plasma.

2.1. Heating device [31]

Induction heating is a long-time known way to heat metals by the magnetic induction of an alternating current (Eddy current) into a conductor. The principle and details of the induction heating technique is very well understood and described for instance in [32].

The device proposed here is not intended to heat the substrate itself directly (although it is the case if the substrate is a conducting material). Instead, a heating susceptor is placed under the substrate. The susceptor is made of thin sheet of a conducting material, preferably with a high melting point and a high Curie point.

The heating device consists in an inductive coil rounding a ferrite block placed under the bottom electrode and a susceptor placed between the bottom dielectric and the substrate. As the bottom electrode is above the inductive coil and under the dielectric, its geometry contains holes to allow the magnetic loops to reach the susceptor. A schematic of the heating device is presented in Fig. 2.

The electrode used (called hollow electrode) is a disk made of a good conductor (Aluminum, 50 mm of diameter) that has a slit from the side to the center to avoid the apparition of Eddy current in the electrode. As the coil is placed underneath the center of the electrode, and has a smaller diameter than the electrode itself, the center of the electrode is a hole of the diameter of the coil, also to avoid heating. The susceptor is placed above the hole in such a way that magnetic loops are perpendicular to it. The thickness of the susceptor is an important parameter since it will affect its resistance through the skin effect and as described in Fig. 2.

The heating device build on this principle uses an alternating current of 17,5 *V* and 4 A at a frequency between 20 and 80 kHz passing through a Litz wire cable wrapped six time around a ferrite core of 20 mm and constituting the heating coil. The susceptor is made of a copper foil of 0.1 mm thick and 25 mm of diameter this configuration allows to reach 573 K in 1 min. The temperature is measured on top of the substrate without the plasma and using a thermocouple K.

The deposited coatings are characterized using X-ray diffraction (Rigaku Ultima IV diffractometer for V_2O_5 coatings and a D8 Advance Eco Brüker diffractometer with Cu kα ($\lambda = 1.5418$ Å) and 1,5° of grazing angle for TiO_2 coatings), X-ray photoelectron spectroscopy (Physical Electronics, PHI 5600 spectrometer using the Mg anode operating at 200 W), and Fourier transform infrared spectroscopy(Nicolet 5700 spectrometer). Commercially available V_2O_5 (J.T.Baker CAS#1314-62-1), VO_2 (Sigma-Aldrich CAS#12036–21-4) and TiO_2 powders (Sigma-Aldrich Product#232033) are used as references.

3. Results

3.1. Vanadium oxide

Using PECVD it has been shown that one could deposit crystalline V_2O_5 at lower temperatures than those used for conventional CVD. Barreca et al. [33] showed that $VO(hfa)_2.H_2O$ in a low pressure PECVD process can deposit V_2O_5 in highly oriented orthorhombic phase at only 423 K, Musschoot et al. got the same temperature for PE-ALD of O_2 and vanadium triisopropoxide oxide [34]. However, such studies were conducted at low pressure. For C*V*D the process usually needs a post-deposition annealing to obtain a crystalline phase or a deposition at high temperature. Piccirillo et al. [35] used $V(acac)_3$ and $VO(acac)_2$ to obtain crystalline VO_x at atmospheric pressure and 773 K, Field et al. [36] used $VOCl_3$ and VCl_4 in an APCVD reactor at 733 K to obtain V_2O_5, Manning et al. [37] deposited VO_x with VCl_4 by APCVD process at

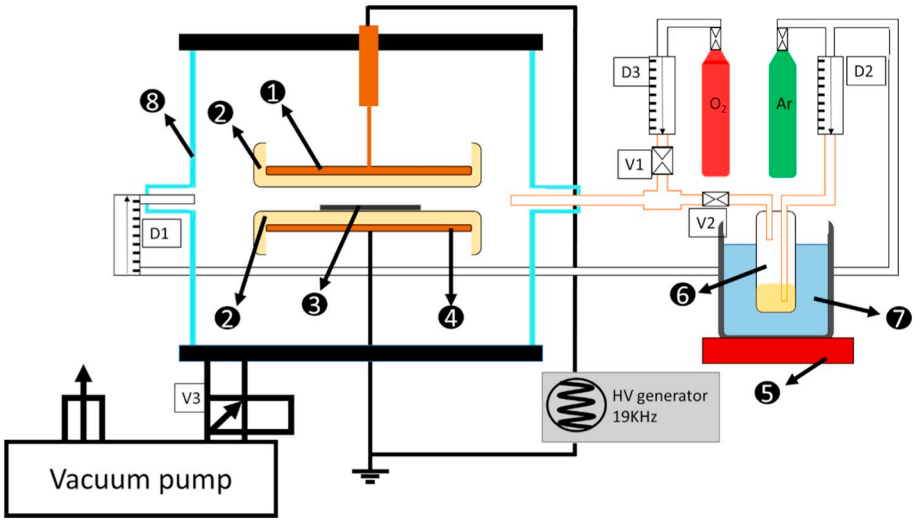

Fig. 1. Schematic of the deposition setup. 1) High voltage electrode; 2) Dielectric; 3) Substrate; 4) Ground electrode; 5) Heating plate; 6) Bubbler; 7) Thermostated water bath; 8) Closed chamber; V1) Dioxygen valve, V2) Precursor valve, V3) Atmospheric pressure equalization valve; D1) Argon main plasma gas flowmeter; D2) Argon carrier flowmeter, D3) Dioxygen flowmeter.

temperatures between 733 K and 833 K, Mathur et al. [38] used low-pressure CVD with VOTP to synthetize VO_x by variating the substrate temperature between 673 K and 973 K.

In this study, starting from *V*OTP as precursor, to reach vanadium oxide, carbon and hydrogen must be removed. A pure Argon discharge leads to the deposition of a coating still contaminated with carbon and the XPS spectrum of the Vanadium peaks (V 2p 3/2 and 1/2) (Fig. 3) reveals the presence of vanadium in the +5 but also in the +4 oxidation state. Their respective binding energies for the V2p 3/2 are 517.2 eV and 515.8 eV. This indicates that vanadium, originally in the +5 state in the precursor is partly reduced by the plasma. Indeed, the V5+ peak represents 60% of the Vanadium peak area when the coating is deposited at 50 W, but only 44% when it is synthesized at 60 W. The shoulder on the high energy side of the O1s peak can be attributed to a carbon-oxygen component coming from the carbon contamination (between 40% and 43% given by the full survey of the coatings between 50 W and 60 W) of the coating due to the absence of oxygen in the gas flow.

Increasing the oxygen pressure in the discharge leads to a decrease of the carbon content, and to a decrease of the $V + 4$ state conjugated with an increase of the V + 5 state. This is clearly visible on the evolution of the XPS spectra (Fig. 4), where the V 2p3/2 peaks shifts towards higher binding energies with increasing $\%O_2$ in the discharge. The high energy shoulder centered at 532,5 eV of the O 1 s peak on the 3% oxygen spectrum is due to the presence of the underneath native silicon oxide layer of the Si substrate.

3.2. Deposition of V_2O_5 in an argon/oxygen discharge, on an inductively heated substrate

Fig. 5 shows the IR spectra of the coatings deposited on substrates heated at various temperatures. At 373 K, the CH and OH bands are clearly identified, as well as the two main bands of *V*=O and O-V-O [39] at 1005 and 810 cm-1 respectively [40]. The presence of CH bands at low temperatures, even with 5% O_2 in the reactor, indicates that the reaction is not complete in these conditions. At 473 K, only the *V*=O and O-V-O bands remain, whereas not C-H nor OH bands are detected anymore. A further increase in temperature leads to a sharpening of the *V*=O band and to a decrease in intensity of the V-O band. A shift of the V=O and V-O bands to higher wavenumbers is also observed, suggesting a higher crystallinity of the V_2O_5 coating and, as suggested by Liedberg et al. [41], this behavior is the mark of a strong anisotropy of the coating, given a greater absorption of the V=O band oriented perpendicular to the surface of the substrate.

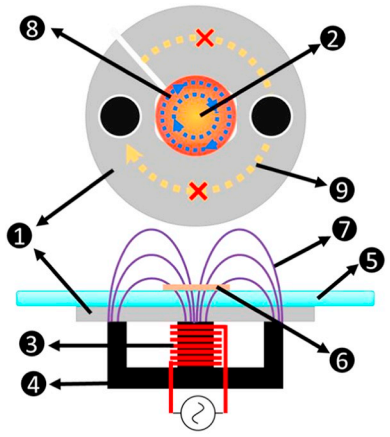

Fig. 2. configuration with hollow electrode. 1) Electrode; 2) Heated zone; 3) induction coil; 4) ferrite core; 5) Dielectric; 6) Susceptor; 7) Magnetic field lines; 8) induced Eddy current (arbitrary direction); 9) impossible current line.

Fig. 6 shows a comparison of the XRD pattern of V_2O_5 deposited on a gold substrate at 573 K and a coating deposited at room temperature and further annealed at 573 K.

From the global XRD diagram, one can already distinguish a better crystallization. Calculating the average size of the crystals from the Scherrer equation, gives values of 13 nm for the coatings obtained by post-annealing, and of 16 nm for the coatings deposited directly at 573 K. These values are however purely indicative, and overestimate for the annealed coating, as it presents very small XRD peaks (see Fig. 6). The average thickness of the coatings, as measured by SEM cross-sectioning, is 56 nm, for a 20 min deposition time. This gives a 2.8 nm/min average deposition rate.

Table 1
Plasma deposition parameters used for the deposition of vanadium oxide and titanium oxide.

	Tot. flux (L/min)	O2 (L/min)	Ar carrier (L/min)	Ar plasma (L/min)	Bubbler temperature (K)	Substrate	Substrate temperature (K)
V2O5	10	0–1	1	8–9	308–313	Si – Al – Au	273–673
TiO2	10	1	0.5–2	7–8.5	333	Si	673

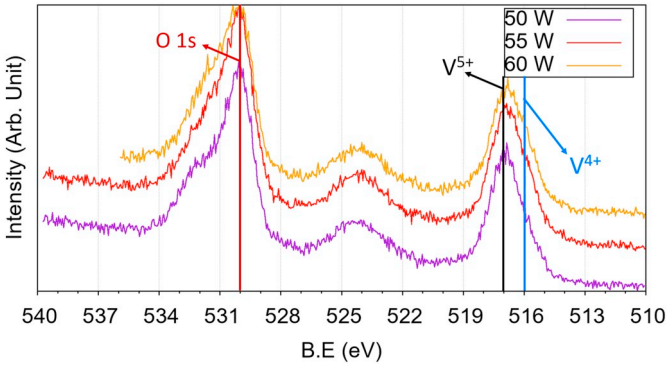

Fig. 3. XPS O1s, *V*2p1/2 and V2p3/2 peaks of coatings deposited from VOTP in an argon discharge at different injected powers. An increase in power leads to an increase in the V + 4 component, indicating partial reduction of the vanadium, originally in the +5 state in the precursor. Conditions are 308 K *VOTP*, 1 L/min argon carrier, 10 L/min total flux and 20 min of deposition time on silicon wafer at 298 K.

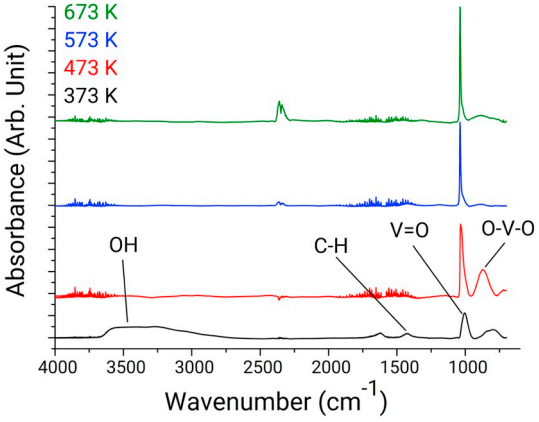

Fig. 5. IR spectra of coatings deposited at different substrate temperatures. The deposition conditions are 30 W, 5% of O_2, VOTP 310 K, 1 L/min of Argon carrier gas, 10 L/min total gas flow, 20 min of deposition time on aluminum 2024 substrate.

A major advantage of in situ, during deposition, heating is that it leads to a better crystallization than post-treatment annealing.

3.3. Deposition of TiO_2

A few studies report de deposition of TiO_2 in the anatase form using atmospheric plasma techniques: [25,42,43]. They use conventional resistive devices to heat the substrate at 573 K [25], 673 K [42] or they use the heat generated by the plasma itself (around 463 K) to obtain a crystalline phase [43].

The deposition of TiO_2 films from TTIP proceed from the same rationale as for vanadium oxide. The TTIP must be fragmented inside the plasma, and the carbonaceous fragments are removed by oxidation, if oxygen is added in the discharge. The experimental procedure for the synthesis of TiO_2 using an atmospheric DBD, TTIP, Ar and oxygen has already been published, as well as the effect of the plasma parameters on the morphology, composition and catalytic activity of the films deposited. They will not be repeated here. Chen, using the same setup, obtained amorphous TiO_2 films, onto room temperature substrates [44,45]. After annealing 2 h at 673 K, small crystals of anatase were formed, and exhibit a photocatalytic activity. This is however a two-step process that leads, as shown for vanadium oxide, to a lower degree of crystallization than direct heating of the substrate.

Fig. 7 a and b show the XRD patterns of TiO_2 coatings deposited on Si and Al at 673 K. It reveals clearly the diffraction peaks of Anatase.

Chen et al. [44,45], on the same setup, with annealing at 673 K but without heating the substrate during deposition, determined an average crystal size of 7.9 nm (based on the (101) diffraction peak of TiO_2). For coatings deposited onto the inductively heated substrate, the average

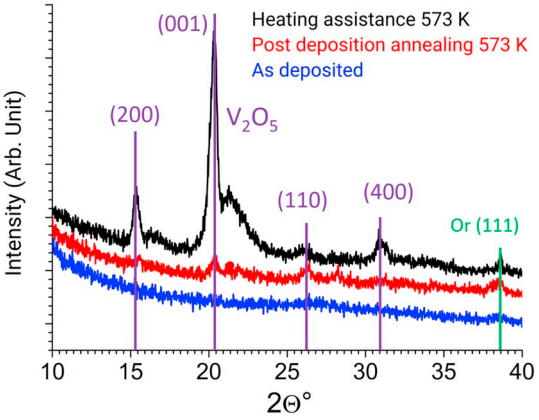

Fig. 6. Deposition of V_2O_5 by atmospheric plasma onto an Au substrate at 10% oxygen in the gas phase, 50 W of power and 310 K of VOTP. Gas flux are 1 L/min of carrier gas, 10 L/min of total flux and 20 min of deposition time on gold substrate.

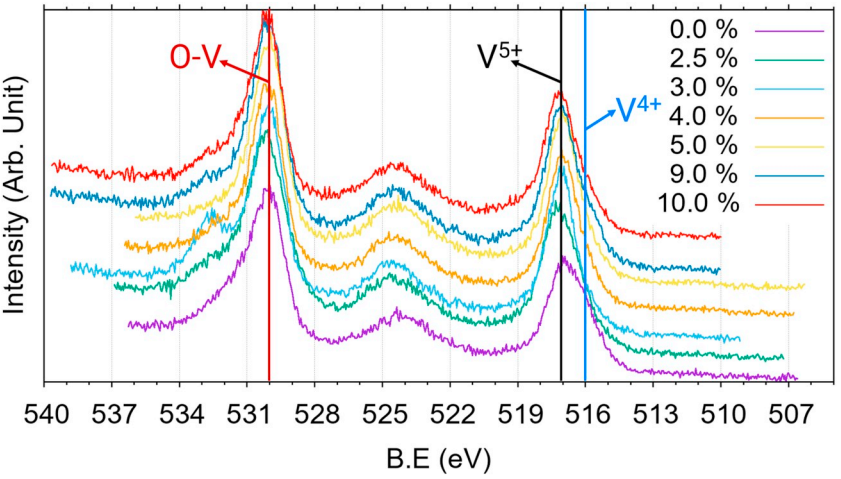

Fig. 4. XPS O1s, *V*2p1/2 and V2p3/2 peaks of coatings deposited from VOTP in an argon/oxygen discharge at different oxygen concentrations. An increase in oxygen leads to a decrease in the V + 4 component. Conditions are 310 K VOTP, 1 L/min argon carrier, 10 L/min total gas flux, O_2 from 0,25 L/min to 1 L/min and 20 min of deposition time on silicon wafer at 298 K.

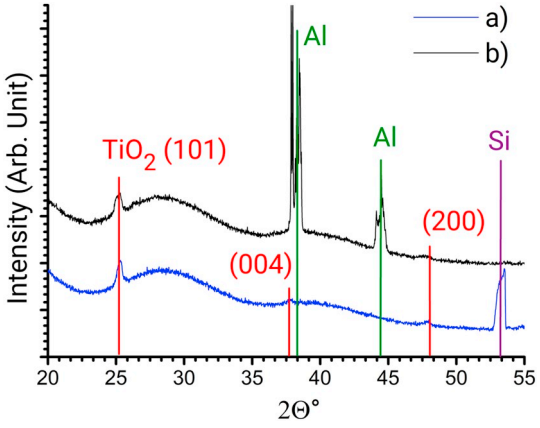

Fig. 7. *a:* XRD diagrams of TiO_2 films deposited onto silicon with the substrate heated at 673 K. Deposition conditions: 0,5 L/min argon carrier, 10% O_2, 10 L/min total flux, 30 W of power and 20 min of deposition.b: XRD diagrams of TiO_2 films deposited onto aluminum, with the substrate heated at 673 K. Deposition conditions: 2 L/min argon carrier, 10% O_2, 10 L/min total flux, 30 W of power and 20 min of deposition .

crystal size is 22.4 nm.

4. Conclusions

Deposition of crystalline coatings using cold atmospheric pressure plasma, once a real challenge due to technological constraints, is facilitated by an inductive heating device of the substrate conveniently located under the dielectric and the bottom electrode. This original setup avoids electrical interferences with the high frequency plasma circuit. It allows fast heating of the substrate, located on top of a dielectric. Crystalline vanadium oxide (V_2O_5) and titanium oxide, anatase (TiO_2) can now easily be grown using an atmospheric DBD, starting from volatile organometallic precursors.

Although the quality of the deposited coatings still remain way below those deposited using low pressure PVD or PECVD techniques, one should remember that the latter ones are much more matured, and where developed since many decades, contrary to the much younger atmospheric pressure thin film deposition.

Acknoweldgements

This work is funded by the EoS (Excellence of Science, Belgian National Research Fund) project “Nitroplasm”, and by the Walloon Region (project Amorpho).

References

[1] P.J. Kelly, R.D. Arnell, Magnetron sputtering: a review of recent developments and applications, Vacuum. 56 (2000) 159–172, https://doi.org/10.1016/S0042-207X(99)00189-X.
[2] J.E. Mahan, Physical Vapor Deposition of Thin Films, Wiley-Interscience, 2000.
[3] S.M. Rossnagel, Thin film deposition with physical vapor deposition and related technologies, J. Vac. Sci. Technol. A Vacuum, Surfaces, Film. 21 (2003) S74–S87, https://doi.org/10.1116/1.1600450.
[4] K. Wasa, S. Hayakawa, Handbook of Sputter Deposition Technology: Principles Technology and Applications, Noyes Publications, 1992.
[5] A. Anders, A review comparing cathodic arcs and high power impulse magnetron sputtering (HiPIMS), Surf. Coat. Technol. 257 (2014) 308–325, https://doi.org/10.1016/j.surfcoat.2014.08.043.
[6] J.E. Greene, Review article: tracing the recorded history of thin-film sputter deposition: from the 1800s to 2017, J. Vac. Sci. Technol. A 35 (2017) 05C204, , https://doi.org/10.1116/1.4998940.
[7] F. Reniers, M.P. Delplancke, A. Asskali, V. Rooryck, O. Van Sinay, Glow discharge sputtering deposition of thin films of ag, Cr, cu, Ni, Pd, Rh and their binary alloys onto NaCl and MgO experimental parameters and epitaxy, Appl. Surf. Sci. 92 (1996) 35–42, https://doi.org/10.1016/0169-4332(95)00198-0.
[8] M. Detroye, F. Reniers, C. Buess-Herman, J. Vereecken, Synthesis and characterisation of chromium carbides, Appl. Surf. Sci. 120 (1997) 85–93, https://doi.org/10.1016/S0169-4332(97)00228-6.
[9] F. Reniers, M. Detroye, S. Kacim, P. Kons, M. Maoujoud, E. Silberberg, M.S. el Begrani, T. Vandevelde, C. Buess-Herman, Synthesis of thin films of Cr, Mo and W carbides and nitrides, in: S.T. Oyama (Ed.), The Chemistry of Transition Metal Carbides and Nitrides, Springer, Netherlands, Dordrecht, 1996, pp. 274–289, , https://doi.org/10.1007/978-94-009-1565-7_14.
[10] U. Kogelschatz, Dielectric-barrier discharges: their history, discharge physics, and industrial applications, Plasma Chem. Plasma Process. 23 (2003) 1–46, https://doi.org/10.1023/A:1022470901385.
[11] E. Silberberg, E. Michel. F. Reniers, C. Buess-Herman, Method for the plasma cleaning of the surface of a material coated with an organic substance and the installation for carrying out said method, World Wide Patent, US No. US10/504, 596, Granted 2010-03-09.
[12] N. Li, Y.L. Wu, J. Hong, I.A. Shchelkanov, D.N. Ruzic, SiO x deposition on polypropylene-coated paper with a dielectric barrier discharge at atmospheric pressure, IEEE Trans. Plasma Sci. 43 (2015) 3205–3210, https://doi.org/10.1109/TPS.2015.2459720.
[13] D. Merche, N. Vandencasteele, F. Reniers, Atmospheric plasmas for thin film deposition: a critical review, Thin Solid Films 520 (2012) 4219–4236, https://doi.org/10.1016/j.tsf.2012.01.026.
[14] F. Massines, N. Gherardi, A. Fornelli, S. Martin, Atmospheric pressure plasma deposition of thin films by townsend dielectric barrier discharge, Surf. Coat. Technol. 200 (2005) 1855–1861, https://doi.org/10.1016/j.surfcoat.2005.08.010.
[15] C. Tendero, C. Tixier, P. Tristant, J. Desmaison, P. Leprince, Atmospheric pressure plasmas: a review, Spectrochim. Acta - Part B At. Spectrosc. 61 (2006) 2–30, https://doi.org/10.1016/j.sab.2005.10.003.
[16] L. Bárdos, H. Baránková, Cold atmospheric plasma: sources, processes, and applications, Thin Solid Films 518 (2010) 6705–6713, https://doi.org/10.1016/j.tsf.2010.07.044.
[17] J. Hubert, C. Poleunis, A. Delcorte, P. Laha, J. Bossert, S. Lambeets, A. Ozkan, P. Bertrand, H. Terryn, F. Reniers, Plasma polymerization of C4Cl6 and C2H2Cl4 at atmospheric pressure, Polym (Guildf). 54 (2013) 4085–4092, https://doi.org/10.1016/j.polymer.2013.05.068.
[18] J. Hubert, N. Vandencasteele, J. Mertens, P. Viville, T. Dufour, C. Barroo, T. Visart De Bocarmé, R. Lazzaroni, F. Reniers, Chemical and physical effects of the carrier gas on the atmospheric pressure PECVD of fluorinated precursors, Plasma Process. Polym. 12 (2015) 1174–1185, https://doi.org/10.1002/ppap.201500025.
[19] B. Nisol, G. Arnoult, T. Bieber, A. Kakaroglou, I. De Graeve, G. Van Assche, H. Terryn, F. Reniers, About the influence of double bonds in the APPECVD of acrylate-like precursors: a mass spectrometry study of the plasma phase, Plasma Process. Polym. 11 (2014) 335–344, https://doi.org/10.1002/ppap.201300176.
[20] B. Nisol, C. Poleunis, P. Bertrand, F. Reniers, Poly(ethylene glycol) films deposited by atmospheric pressure plasma liquid deposition and atmospheric pressure plasma-enhanced chemical vapour deposition: process, chemical composition analysis and biocompatibility, Plasma Process. Polym. 7 (2010) 715–725, https://doi.org/10.1002/ppap.201000023.
[21] J. Hubert, J. Mertens, T. Dufour, N. Vandencasteele, F. Reniers, P. Viville, R. Lazzaroni, M. Raes, H. Terryn, Synthesis and texturization processes of (super)-hydrophobic fluorinated surfaces by atmospheric plasma, J. Mater. Res. 30 (2015) 3177–3191, https://doi.org/10.1557/jmr.2015.279.
[22] A. Demaude, C. Poleunis, E. Goormaghtigh, P. Viville, R. Lazzaroni, A. Delcorte, M. Gordon, F. Reniers, Atmospheric pressure plasma deposition of hydrophilic/phobic patterns and thin film laminates on any surface, Langmuir. (2019), https://doi.org/10.1021/acs.langmuir.9b00493 acs.langmuir.9b00493.
[23] A. Batan, F. Brusciotti, I. De Graeve, J. Vereecken, M. Wenkin, M. Piens, J.J. Pireaux, F. Reniers, H. Terryn, Comparison between wet deposition and plasma deposition of silane coatings on aluminium, Prog. Org. Coat. (2010) 126–132, https://doi.org/10.1016/j.porgcoat.2010.04.009.
[24] D. Merche, C. Poleunis, P. Bertrand, M. Sferrazza, F. Reniers, Synthesis of polystyrene thin films by means of an atmospheric-pressure plasma torch and a dielectric barrier discharge, IEEE Trans. Plasma Sci. 37 (2009) 951–960, https://doi.org/10.1109/TPS.2009.2014165.
[25] R. Kawakami, M. Niibe, Y. Nakano, Y. Araki, Y. Yoshitani, C. Azuma, T. Mukai, Characteristics of TiO2 thin films surfaces treated by O2 plasma in dielectric barrier discharge with the assistance of external heating, Vacuum. 152 (2018) 265–271, https://doi.org/10.1016/j.vacuum.2018.03.051.
[26] H. Jerominek, Vanadium oxide films for optical switching and detection, Opt. Eng. 32 (2006) 2092, https://doi.org/10.1117/12.143951.
[27] D.K. Louie, Handbook of sulphuric acid manufacturing, DKL Engineering, 2 nnd edition, 2008.
[28] I.P. Parkin, R. Binions, C. Piccirillo, C.S. Blackman, T.D. Manning, Thermochromic coatings for intelligent architectural glazing, J. Nanopart. Res. 2 (2009) 1–20, https://doi.org/10.4028/www.scientific.net/jnanor.2.1.
[29] A. Mantoux, H. Groult, E. Balnois, P. Doppelt, L. Gueroudji, Vanadium oxide films synthesized by CVD and used as positive electrodes in secondary Lithium batteries, J. Electrochem. Soc. 151 (2004) A368–A373, https://doi.org/10.1149/1.1641037.
[30] A. Tiwari, I. Mondal, S. Ghosh, N. Chattopadhyay, U. Pal, Fabrication of mixed phase TiO 2 heterojunction nanorods and their enhanced photoactivities, Phys. Chem. Chem. Phys. 18 (2016) 15260–15268, https://doi.org/10.1039/c6cp00486e.
[31] A. Remy, F. Reniers, Dielectric Barrier Discharge Plasma Reactor and Method for Plasma-Enhanced Vapor Deposition, European patent application, 2019 EP19187406.4.
[32] V. Rudnev, D. Loveless, R.L. Cook, Handbook of Induction Heating, 2nd. ed, CRC Press, 2017, https://doi.org/10.1201/9781315117485.
[33] D. Barreca, L. Armelao, F. Caccavale, V. Di Noto, A. Gregori, G.A. Rizzi, E. Tondello,

Highly oriented V2O5 nanocrystalline thin films by plasma-enhanced chemical vapor deposition, Chem. Mater. 12 (2000) 98–103, https://doi.org/10.1021/cm991095a.
[34] J. Musschoot, D. Deduytsche, H. Poelman, J. Haemers, R.L. Van Meirhaeghe, S. Van den Berghe, C. Detavernier, Comparison of thermal and plasma-enhanced ALD/CVD of vanadium pentoxide, J. Electrochem. Soc. 156 (2009) P122, https://doi.org/10.1149/1.3133169.
[35] C. Piccirillo, R. Binions, I.P. Parkin, Synthesis and functional properties of vanadium oxides: V2O3, VO2 and v2O5 deposited on glass by aerosol-assisted CVD, Chem. Vap. Depos. 13 (2007) 145–151, https://doi.org/10.1002/cvde.200606540.
[36] M.N. Field, I.P. Parkin, Atmospheric pressure chemical vapour deposition of vanadium(v) oxide films on glass substrates from reactions of VOCl3 and VCl4 with water, J. Mater. Chem. 10 (2000) 1863–1866, https://doi.org/10.1039/b002132f.
[37] T.D. Manning, I.P. Parkin, M.E. Pemble, D. Sheel, D. Vernardou, Intelligent window coatings: atmospheric pressure chemical vapor deposition of tungsten-doped vanadium dioxide, Chem. Mater. 16 (2004) 744–749, https://doi.org/10.1021/cm034905y.
[38] S. Mathur, T. Ruegamer, I. Grobelsek, Phase-selective CVD of vanadium oxide nanostructures, Chem. Vap. Depos. 13 (2007) 42–47, https://doi.org/10.1002/cvde.200606578.
[39] I.L. Botto, M.B. Vassallo, E.J. Baran, G. Minelli, IR spectra of VO2 and V2O3, Mater. Chem. Phys. 50 (1997) 267–270, https://doi.org/10.1016/S0254-0584(97)01940-8.
[40] Y. Yang, F. Teng, Y. Kan, L. Yang, W. Gu, J. Xu, Y. Zhao, X. Du, M. Ren, Controllable synthesis of 'l'-shaped V2O5 and the improved adsorption capacity by fluorine, CrystEngComm. 18 (2016) 3064–3078, https://doi.org/10.1039/c6ce00079g.
[41] B. Liedberg, B. Ivarsson, I. Lundström, W.R. Salaneck, Fourier transform infrared reflection absorption spectroscopy (FT-IRAS) of some biologically important molecules adsorbed on metal surfaces, in: B. Lindman, G. Olofsson, P. Stenius (Eds.), Surfactants, Adsorption, Surface Spectroscopy and Disperse Systems, Progress in Colloid & Polymer Science book series, vol. 75, Springer, 2007, pp. 67–75, , https://doi.org/10.1007/bfb0114307.
[42] X.W. Zhang, G.R. Han, Microporous textured titanium dioxide films deposited at atmospheric pressure using dielectric barrier discharge assisted chemical vapor deposition, Thin Solid Films 516 (2008) 6140–6144, https://doi.org/10.1016/j.tsf.2007.11.019.
[43] L.H. Nie, C. Shi, Y. Xu, Q.H. Wu, A.M. Zhu, Atmospheric cold plasmas for synthesizing nanocrystalline anatase TiO2 using dielectric barrier discharges, Plasma Process. Polym. 4 (2007) 574–582, https://doi.org/10.1002/ppap.200600212.
[44] Q. Chen, Q. Liu, J. Hubert, W. Huang, K. Baert, G. Wallaert, H. Terryn, M.P. Delplancke-Ogletree, F. Reniers, Deposition of photocatalytic anatase titanium dioxide films by atmospheric dielectric barrier discharge, Surf. Coat. Technol. 310 (2017) 173–179, https://doi.org/10.1016/j.surfcoat.2016.12.077.
[45] Q. Chen, Q. Liu, A. Ozkan, B. Chattopadhyay, G. Wallaert, K. Baert, H. Terryn, M.P. Delplancke-Ogletree, Y. Geerts, F. Reniers, Atmospheric pressure dielectric barrier discharge synthesis of morphology-controllable TiO2 films with enhanced photocatalytic activity, Thin Solid Films 664 (2018) 90–99, https://doi.org/10.1016/j.tsf.2018.08.025.